Energy 135 (2017) 91–100

Contents lists available at ScienceDirect

Energy

journal homepage: www.elsevier.com/locate/energy

The influence of driving cycle characteristics on the integrated optimization of hybrid energy storage system for electric city buses

Ziyou Song [a, b], Jun Hou [b], Shaobing Xu [a], Minggao Ouyang [a], Jianqiu Li [a, c, *]

[a] State Key Laboratory of Automotive Safety and Energy, Tsinghua University, Beijing 100084, PR China
[b] Department of Electric Engineering and Computer Science, University of Michigan, Ann Arbor, MI 48109, USA
[c] Collaborative Innovation Center of Electric Vehicles in Beijing, Beijing 100081, PR China

ARTICLE INFO

Article history:
Received 20 March 2017
Received in revised form
25 May 2017
Accepted 16 June 2017
Available online 20 June 2017

Keywords:
Electric vehicle
Hybrid energy storage system
Component sizing
Fuzzy pattern recognition
Driving cycle characteristics
Integrated optimization

ABSTRACT

This paper analyzes the influence of different driving cycles on the integrated optimization of hybrid energy storage system, including the optimization of supercapacitor size and energy management strategy for the electric vehicle application. The driving cycle is divided into micro-trips, and a fuzzy pattern recognition algorithm is proposed to distinguish different micro-trips within a driving cycle. The intensity factor indicates how intensely the micro-trip drains energy from the hybrid energy storage system. The distribution of each driving cycle is analyzed by the probability density function. The integrated optimization of the hybrid energy storage system is conducted based on four driving cycles. Simulation results show that for different driving cycles, the optimal supercapacitor size and the on-line energy management strategy are directly determined by the maximum intensity factor. The driving cycles with similar maximum intensity factors can use same amount of supercapacitor modules and employ the same on-line energy management strategy. Therefore, the optimization results can be easily generalized to practical bus lines.

© 2017 Elsevier Ltd. All rights reserved.

1. Introduction

Electric vehicles (EVs) are receiving considerable attention as effective solutions for energy and environmental problems [1]. Lithium battery is widely used in EV applications due to its high energy density and safety. However, batteries used in EVs often perform frequent charge and discharge operations [2], which have an adverse effect on battery life [3]. Therefore the hybrid energy storage system (HESS), which combines the functionalities of supercapacitors (SCs) and batteries [4], can be an effective solution to extend battery life span [5]. To effectively protect the battery by using the SC, the HESS topology, the SC size, and the energy management strategy (EMS) should be optimized [6]. In terms of the HESS topologies, the optimization results in Ref. [7] show that the semi-active HESS, which only employs one DC/DC converter, offers a good balance between performance and system cost. Hence, a typical semi-active HESS, as shown in Fig. 1, is adopted in this study.

For a definite HESS topology, the optimal sizing and the EMS optimization processes should be considered simultaneously since these two issues are integrated [6]. In Ref. [6], dynamic programming (DP) algorithm was used to derive the optimal SC size and EMS of a HESS equipped in an electric city bus. One important issue that emerges from the simulation results is that different driving cycles significantly impact the SC sizing result and the EMS optimization result. However, the integrated optimization process needs hundreds of hours only for one driving cycle because the computational cost of DP is high. It is difficult to generalize the optimization result in practical driving cycles. Thus, a simple criterion is needed to justify whether the optimization results based on a standard driving cycle can be generalized to a new driving cycle without conducting DP when its statistical driving data is known.

To the best of our knowledge, the influence of different driving cycles on HESS optimization has not been reported in the existing literature. Most approaches used for the HESS optimization are based on a fixed driving cycle [8], and therefore do not deal with the variability in the driving situation [9]. For example, Wang et al. proposed a novel co-estimator to estimate the model parameters and state-of-charge simultaneously [10]. Yu et al. proposed an innovative real time EMS design approach for a fast charging

* Corresponding author. State Key Laboratory of Automotive Safety and Energy, Tsinghua University, Beijing 100084, PR China.
E-mail addresses: ziyou.song@qq.com (Z. Song), lijianqiu@tsinghua.edu.cn (J. Li).

http://dx.doi.org/10.1016/j.energy.2017.06.096
0360-5442/© 2017 Elsevier Ltd. All rights reserved.

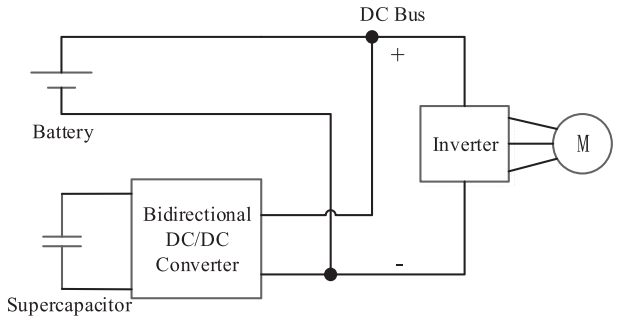

Fig. 1. The typical semi-active HESS topology.

electric urban bus with HESS [11]. The real-world driving cycle may significantly influence the vehicle performance when compared to the one under standard driving cycles [12]. The intelligent EMS for hybrid electric vehicles (HEVs) and plug-in hybrid electric vehicles (PHEVs), which gives appropriate consideration to the driving information, has been widely studied in the past decades. To be specific, by using the on-board global positioning systems (GPSs), Gong et al. proposed the two-scale DP algorithm for a PHEV associated with the driving cycle modeling based on intelligent transportation systems (ITS) [13]. Gu et al. analyzed the past driving conditions periodically and recognized the driving patterns, and they accordingly chose different equivalence factors for the equivalent consumption minimization strategy (ECMS) [14]. Jeon et al. selected 6 driving patterns and optimized parameters of the EMS for each pattern via off-board calculation. By using artificial neural networks, driving pattern recognition was conducted in real-time control process [15]. Different from Jeon, Lin et al. used a simple rule-based strategy to recognize the driving pattern instead of using artificial neural networks [16]. Wu et al. proposed a fuzzy EMS based on driving cycle recognition to improve the fuel economy of a parallel HEV [17]. Reza et al. proposed an intelligent EMS based on a fuzzy pattern recognition method [18].

One drawback to these approaches is their large computational cost for on-line implementation. More important, the system parameters may not be optimal because the system sizing process is not considered in the aforementioned optimization processes. To be specific, different driving cycles not only require different control strategies but also different component sizes to achieve the best performance. As shown in Fig. 2, the integrated optimization of HESS first obtains the optimal component sizes for different driving cycles. Based on the optimal sizing results, the optimal EMS for different driving cycles can be acquired. There is a one-to-one correspondence between the driving cycle, the optimal component size, and the optimal EMS. To be specific, for the driving cycle A, only the size A is optimal, and it is certainly wrong if the optimization is conducted based on optimal size B or C. Furthermore, optimal EMS B or C cannot be used in the optimization for driving cycle A, even though the optimal size A is employed. However, the existing literature only focuses on the influence of different driving cycles on the EMS optimization results, and the optimal sizing process is skipped. This means that the driving cycle may be linked to the improper EMS, as shown in Fig. 2, resulting in the inaccurate result. Thus the influence of different driving cycles on the optimal sizing process cannot be neglected in the optimization.

Building upon the prior work, this paper investigates the relationship between driving cycle characteristics and the integrated optimization results of HESS, including both optimization results for SC size and on-line EMS. The influence of different driving cycles on the HESS optimal sizing process is properly considered. A fuzzy pattern recognition is proposed to evaluate the micro-trip intensity, which describes how intense the power demand profile is. Generally, the intense power profile contains high power demand and lasts for a long time, indicating that it demands a large amount of energy from HESS at high power rates. The intense micro-trip will increase both the electricity and battery degradation costs. Hence, a plenty of SC modules are needed to decrease the operation cost. In this paper, four driving cycles, including the typical China Bus Driving Cycle (CBDC), the Urban Dynamometer Driving Schedule (UDDS), and two real bus driving cycles in Zhengzhou, China, are compared. The integrated optimization problem is solved by using the DP approach, which is one of the most widely used global optimization methods, for the four driving cycles. The DP approach is adopted to derive the best solutions under different driving cycles. Only in this way, the influence of driving cycle characteristics on SC sizing and EMS development can be accurately analyzed. The simulation results show that the optimal SC size and on-line EMS depend on the maximum intensity factor of the driving cycle. The driving cycles, which have a similar maximum intensity factor, can use the same number of SC modules and employ the same on-line EMS. Thus, without repeating the DP process, the optimization result can be generalized to real bus lines because the city bus route is fixed and its driving data is convenient to be obtained.

This paper is organized as follows: In Section 2, the dynamic model of the HESS is illustrated. Section 3 presents a detailed description of fuzzy pattern recognition. In Section 4, the integrated optimization process is presented. Further analysis of the driving cycle influence on the HESS optimization result is illustrated in Section 5. Conclusions are presented in Section 6.

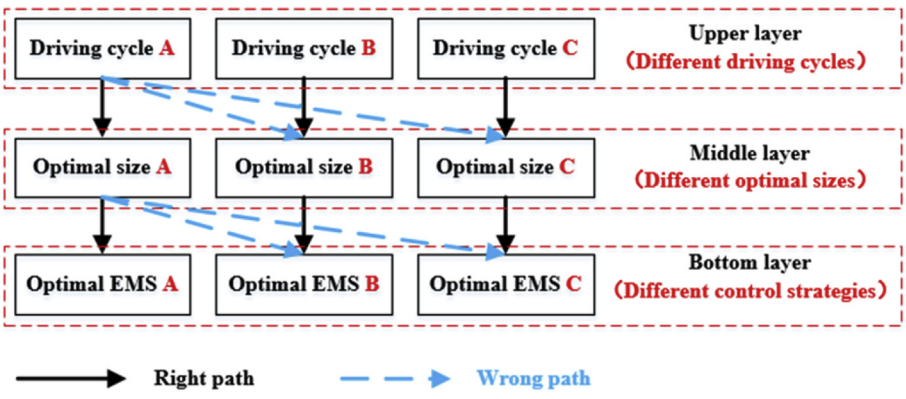

Fig. 2. The integrated optimization schematic of HESS.

2. System modeling

Before analyzing the proposed algorithm, the HESS model and the EV dynamic model are introduced in this section.

2.1. Hybrid energy storage system dynamics

The configuration of the HESS employed in this paper is shown in Fig. 1. The bidirectional DC/DC converter used to interface the SC with the DC bus is the only actuator for the EMS. The supervisor controller gathers the information of SCs, batteries, and the powertrain to calculate the SC demand power P_{SC} and control the SC power via the DC/DC converter [6]. The relationship between the powertrain power demand P_{demand}, P_{SC}, the battery power P_{bat}, and the DC/DC converter power $P_{DC/DC}$ can be determined, as presented in Ref. [6].

The detailed information about the adopted SC module and battery cell is presented in Ref. [6]. The HESS optimization process is over a long time interval (several minutes for a driving cycle). Therefore, the *Rint-Capacity* model is adopted to represent the characteristics of the SC pack, and the battery behavior is represented by the *Rint* model. For the convenience of readers, the parameters of the battery cell and the SC module are listed in Tables 1 and 2, respectively.

The dynamic battery capacity degradation model used in this study is shown in Eq. (1) [6].

$$Q_{loss} = 0.0032e^{-\left(\frac{15162-1516C\_Rate}{RT_{bat}}\right)}(A_h)^{0.824}, \quad (1)$$

where Q_{loss} is the percentage of battery capacity loss, R is the gas constant (J/(mol K)), T_{bat} is the absolute temperature (K), A_h is the Ah-throughput, and C_Rate is the battery discharge rate. This model is based on a semi-empirical model [19], and it is verified to be accurate in the dynamic process [6].

2.2. Electric vehicle modeling

The main parameters of the city bus are listed in Table 3, and the basic dynamic model of the bus is as also provided in Ref. [6]. Most energy of the HESS is stored in the battery pack since the energy density of SC is low. The Chinese government requires the mileage of electric bus to be more than 150 km at a constant speed v_0 (40 km/h) on a flat road (α equals to 0) [21]. Therefore, in the following analysis, the number of battery cell is fixed to 600 (5 parallel and 120 series connection) [6].

3. The integrated optimization of hybrid energy storage system

The integrated optimization means that the SC sizing and EMS development are considered simultaneously since they influence each other [6]. To be specific, in the SC sizing process, the EMS of all HESS candidates (with different amount of SC modules) are optimized by using the DP approach. The potential of all HESS candidates on reducing the battery degradation is exploited. Therefore the best HESS can be found by selecting the minimum operation cost.

The DP approach is adopted to understand the maximum benefits that the global optimization can bring along the entire driving cycle. The SC voltage V_{SC} is the primary state in the DP process, and V_{SC} is discretized to 250 states in its operation range (it is generally considered that 75% energy in SC can be used). The HESS operation cost at any discrete time k, including the electricity and battery degradation costs, is calculated as follows:

$$\text{Minimize}\left\{\sum_{k=1}^{k=k_{max}}\frac{[Cost_{bat,loss}(k)+Cost_{ele}(k)]}{L_c}\right\}, \quad (2)$$

where

$$Cost_{bat,loss}(k)=\frac{V_{bat\_cell}C_{bat}price_{bat}}{0.2\times1000}\times\left[7.73\times10^{-4}\frac{|I_{bat}(k)|T_s}{3600M_{bat}}e^{-\left(\frac{15162-1516C.Rate}{0.824RT_{bat}}\right)}Q_{loss}(k-1)^{-0.2136}\right].$$

$$Cost_{ele}(k)=\frac{price_{ele}\cdot T_s}{3600}[P_{SC}(k)+P_{bat}(k)]$$

T_s is the sample time and set to 1s to reduce the computational cost, $Cost_{bat,\,loss}(k)$ is the battery degradation cost from instant $k-1$ to k, $price_{bat}$ and $price_{ele}$ are the battery and electricity prices which are set to 2000RMB/kW h and 0.8RMB/kW h, M_{bat} is the parallel number of the battery cell and set to 5, $Cost_{ele}(k)$ is the electricity cost, and L_c is the driving cycle mileage. In addition, the SC price is set to 100.5kRMB/kW h [20]. The cost function shown in Eq. (2) has been designed and used in previous work, so the detailed

Table 1
Parameters of the SC module.

Parameter	Value
Maximal voltage (V)	27
Capacity (F)	140
Stored energy (Wh)	14.2
Specific power (W/kg)	1700
Specific energy (Wh/kg)	2.3
Operation temperature range (°C)	−40 to 65

Table 2
Parameters of the battery cell.

Parameter	Value
Cell nominal voltage (V)	3.2
Cell capacity (Ah)	60
Cell stored energy (kWh)	0.192
Cell mass (kg)	~2
Discharging temperature range (°C)	−20 to 55
Charging temperature range (°C)	0 to 45
Recommended SOC usage window (%)	10 to 90

Table 3
Parameters of the city bus.

Parameter	Value
m, Vehicle mass (kg)	15500
Vehicle length (m)	12
R, Wheel radius (m)	0.5
g, Gravity acceleration (m s^{-2})	9.8
C_D, Air drag coefficient	0.7
A, Front area (m^2)	7.5
ρ, Air density (kg.m^{-3})	1.29
η_{md}, Motor efficiency (%)	85
η_T, Transmission efficiency (%)	90
η_r, Regenerative braking efficiency (%)	65
$\eta_{DC/DC}$, DC/DC converter efficiency (%)	85
η_{HESS}, HESS average efficiency (%)	95
DC bus voltage (V)	300–600

information can be referred to Ref. [6].

The minimum cost along the entire driving cycle can be found by proceeding backwards. The SC initial voltage is set to 90% of its maximum value. The detailed process of the integrated optimization can be referred to Ref. [6]. For readers' convenience, the exchange rate between Chinese and US dollars is about 6.9 [21].

4. The fuzzy pattern recognition algorithm

Four driving cycles are investigated in this paper, which are CBDC, UDDS, and two real bus driving cycles in Zhengzhou city, denoted as ZZ #1 and ZZ #2, which were obtained by the bus company in Zhengzhou. These real world driving cycles are necessary to evaluate the EV performance. The speed and corresponding power demand profiles of the aforementioned driving cycles are shown in Fig. 3.

Driving pattern is generally defined in terms of the vehicle speed profile in a particular environment [22]. The driving cycle is comprised of micro-trips, which are excursions between two successive instants at which the EV stops, e.g., CBDC includes 14 micro-trips. The characteristic of a driving cycle is dependent on its micro-trip features. The basic information of different driving cycles is compared in Table 4. The data of ZZ #1 and ZZ #2 are obtained from real-world data of public buses running in Zhengzhou, China. They have short time durations but high acceleration when compared to CBDC. Thus high maximum power occurs in both ZZ #1 and ZZ #2, although their maximum speeds are relatively low. The UDDS has a higher maximum speed than the ones occurring in the other driving cycles. As a result, the maximum power demand in the UDDS is high, meaning that the UDDS is a severe scenario to the HESS. To be specific, SC will be exhausted frequently under high power demand conditions since SC has a low energy density, leading to the fact that the battery should supply the demand power individually. This will dramatically increase the battery degradation cost, especially under the high power and long-duration conditions.

Table 4
Basic parameters of the driving cycles.

Parameter	CBDC	UDDS	ZZ#1	ZZ#2
Cycle time (s)	1305	1370	939	692
Maximal speed (km/h)	60	92	50	46
Maximal charge power demand (kW)	131	192	200	124
Maximal discharge power demand (kW)	173	338	273	274
Micro-trip number	14	17	12	7
Whole driving distance (km)	5.84	11.99	4.31	4.04
Maximal acceleration (m/s^2)	0.83	1.47	3.43	3.42
Average acceleration (m/s^2)	0.15	0.32	0.34	0.34
Maximal deceleration (m/s^2)	−1.06	−1.47	−3.98	−1.48
Average deceleration (m/s^2)	−0.41	−0.50	−0.54	−0.46

In order to evaluate the driving cycle intensity, the fuzzy pattern recognition is proposed in this paper to extract the characteristics parameter of the micro-trip. The fuzzy logic method has been widely used in pattern recognition and energy management applications of HESS due to its convenience [23]. An algorithm that can convert the linguistic control strategy based on expert

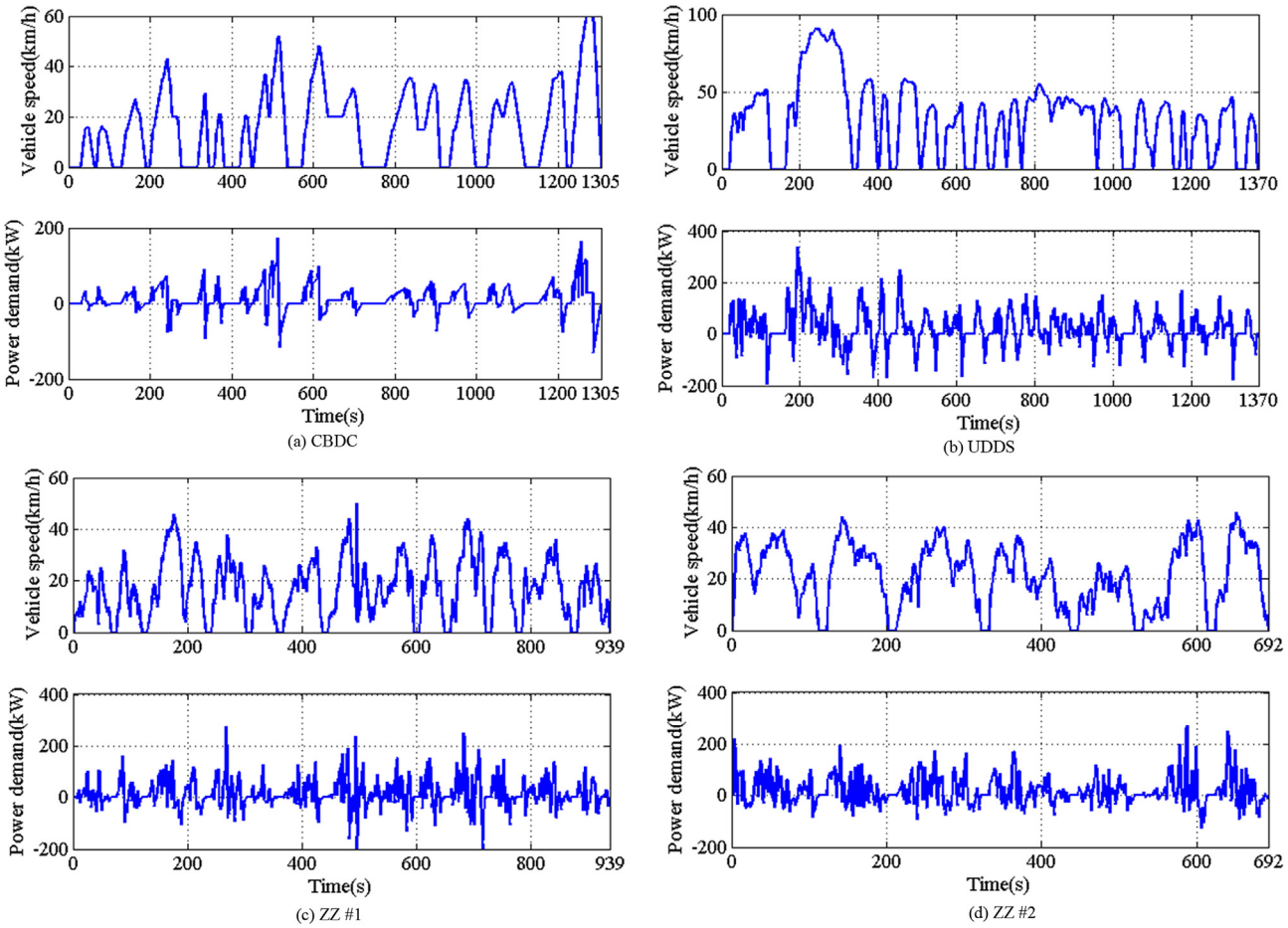

Fig. 3. The speed and power profiles of four driving cycles.

knowledge into an automatic control strategy is provided by fuzzy logic method [24]. The fuzzy pattern recognition algorithm used in this study includes two inputs: the demand energy E_d and the maximum discharge power P_{max}, and one output: the intensity factor λ of the micro-trip. The demand energy, as shown in Eq. (3), is a good index to describe the trend of SC exhaustion. And the maximum discharge power is a good index to evaluate the battery degradation rate since it exponentially increases with *C_Rate*, as shown in Eq. (1).

$$E_d = \int_{t_0}^{t_f} P_{demand}(t) \cdot dt, \tag{3}$$

where t_0 is the start instant, and t_f is the end instant of the micro-trip. The membership functions of inputs and output are shown in Fig. 4.

The 26 rules for the proposed fuzzy pattern recognition are listed in Table 5, where s1, s2, m, h1, h2 represent small1, small2, medium, high1, and high2. The numeric value of each rule indicates its weight parameter. Actually, E_d is the primary input of the fuzzy pattern recognition and P_{max} is an auxiliary input because SC can supply very high power in a short period. The micro-trip with a low E_d and a high P_{max} has barely impact on the HESS. The energy shortage in SC pack occurs only when E_d is high. And in this case, the increase rate of the battery degradation cost is proportional to P_{max}. As a result, the intensity factor λ, which varies from 0 to 1, mainly depends on E_d.

To present the λ distribution of the driving cycle, the probability density function is used. The probability density statistics of four studied driving cycles is shown in Fig. 5, which shows that significant difference occurs in the λ distributions of different driving cycles. Furthermore, all λ values of CBDC, ZZ #1, and ZZ #2 are below 0.5, while there is a λ value in UDDS higher than 0.8. This reveals that UDDS contains much more intense micro-trip than the other driving cycles do, which may dramatically impact the HESS optimization result. This characteristic is important and will be illustrated in detail in Section 5.

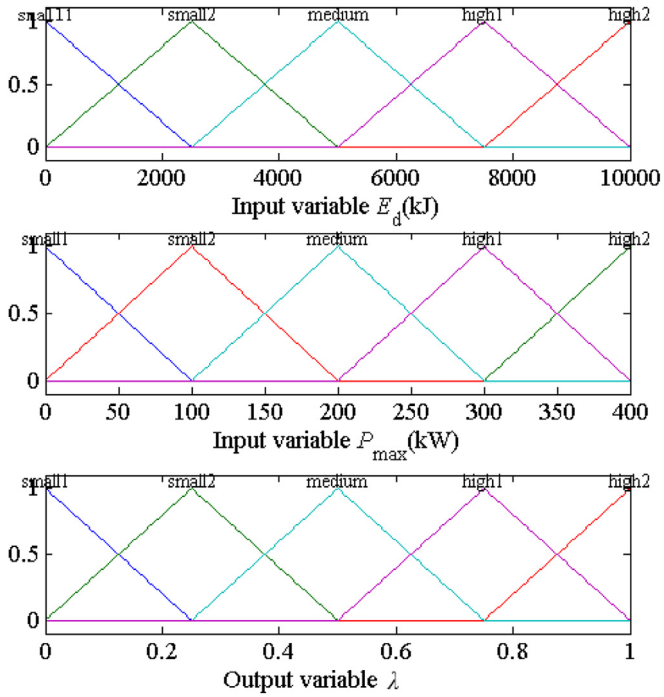

Fig. 4. Memberships of the inputs and output in the FPR algorithm.

Table 5
Rules of the FPR.

E_d	P_{max}	λ	Weight	E_d	P_{max}	λ	Weight
h2	h2	h2	1	m	h1	h1	0.5
h1	h2	h2	1	m	m	h1	0.5
m	h2	h1	1	m	s2	h1	0.5
s2	h2	s2	1	m	s1	m	0.5
s1	h2	s1	1	s2	s2	s2	1
h2	m	h2	1	s2	m	s2	1
h2	s2	h2	0.5	s2	s1	s2	1
h2	s1	h1	1	s2	h1	s2	1
h2	h1	h2	1	s2	s1	s2	0.5
h1	m	h2	0.5	s1	h1	s1	1
h1	s2	h2	0.5	s1	m	s1	1
h1	h1	h2	0.5	s1	s1	s1	1
h1	s1	h1	0.5	s1	s2	s1	1

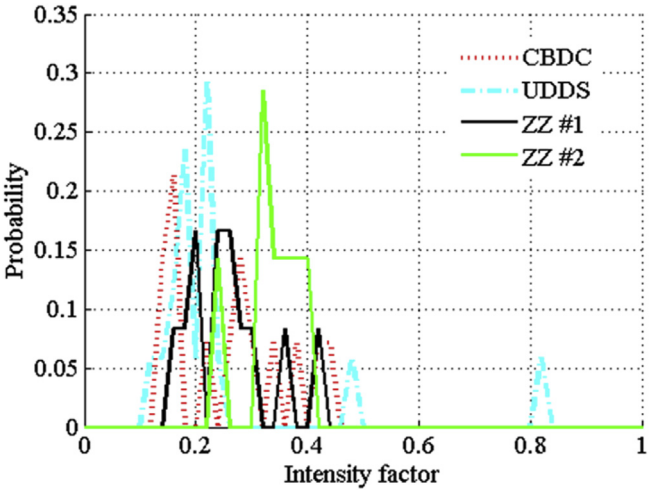

Fig. 5. The λ distributions of four studied driving cycles.

5. Simulation results and analysis

In this section, the proposed algorithm is adopted in the simulation and the results are presented. The simulation is conducted in Matlab/Simulink.

5.1. Optimization results under four driving cycles

The HESS integrated optimization for each studied driving cycle is conducted by using DP approach. The detailed process of the integrated optimization is presented in Ref. [25]. In the SC sizing process, the parallel number of the SC module M_{SC} varies from 1 to 6, and the series number N_{SC} varies from 15 to 30. The minimum operation cost of each HESS candidate over the entire driving cycle can be sought by the DP approach. The SC sizing results for these four driving cycles are shown in Fig. 6.

As shown in Fig. 6, among the four driving cycles, the operation cost of CBDC is the lowest, while the one of ZZ #1 is the highest. The reason is that ZZ #1 and ZZ #2 have high acceleration rates and low average speed, which results in a high electricity cost and a low mileage. Thus their operation cost is relatively high. In addition, the SC sizing results of all driving cycles have the same trend. To be specific, the operation cost can be rapidly reduced initially with an increase in the SC cost; however, the effect of increasing the SC

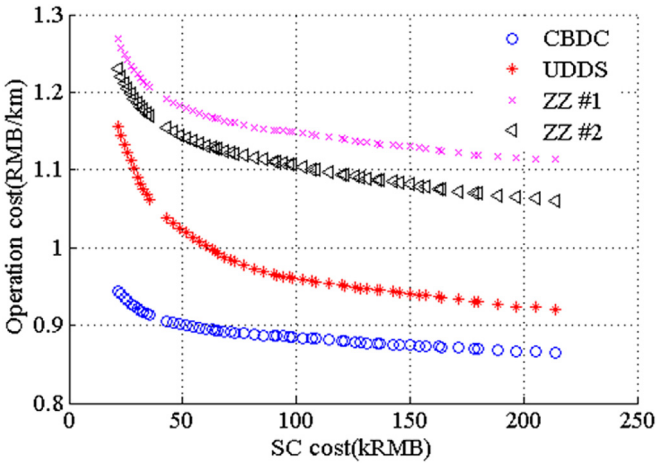

Fig. 6. The SC sizing results.

usage on reducing the HESS life cycle cost is not apparent when SC cost is high. Consequently, the HESS candidate occurring in the transition area can be regarded as the optimal solution. The operation cost as a function of SC cost can be split into two regions. To find the optimal candidate, the reduction rate δ of the HESS operation cost by increasing the SC amount can be defined as

$$\delta = -\frac{oc_i - oc_j}{C_i - C_j}, \tag{4}$$

where oc_i/oc_j are the operation cost corresponding to the ith/jth solutions, and C_i/C_j are initial SC costs of the ith/jth solutions. The relationship between δ and SC cost for different driving cycles are shown in Fig. 7.

As shown in Fig. 7, all δ curves can be divided into two regions. It can be considered beneficial to reduce the operation cost by increasing the SC in region #1, because δ decreases significantly with a slight increase in the SC cost. In region #2, δ almost converges to be a constant value. Therefore, the SC cost on the boundary of the two regions can be considered as the optimal solution. CBDC, ZZ #1, and ZZ #2 have similar optimal solutions (~70 kRMB), in addition, UDDS demands more SC modules (~100 kRMB) than the other driving cycles do since UDDS contains an intense micro-trip. So the optimal SC amount corresponding to the CBDC, ZZ #1, and ZZ #2 is 50 (71.4 kRMB, $M_{SC} = 2$, and $N_{SC} = 25$). In addition, 72 SC modules (102.8 kRMB, $M_{SC} = 3$, and $N_{SC} = 24$) are optimal regarding to UDDS. The sizing result shows that more SCs are needed to reduce the HESS operation cost under the UDDS.

DP approach can find the global optimization solution, but it is difficult to be implemented in practical applications due to its high computational cost. The on-line EMS can be designed based on DP result [6]. The relationship between P_{demand} and P_{SC} should be carefully examined to design the on-line EMS (P_{bat} is determined by P_{demand} and P_{SC}). The HESS DP results under different driving cycles are shown in Fig. 8. As shown in Fig. 8 (a), the DP result under CBDC shows that the relationship between P_{demand} and P_{SC} is explicit and can be divided into three sections. Section #1 indicates that the SC tends to absorb all regenerative energy to avoid the battery frequent charge operations under regenerative braking conditions. Section #2 and Section #3 show that on the traction condition, the SC does not support any power when P_{demand} is less than a definite threshold P_{min}. Additionally, when P_{demand} exceeds P_{min}, the battery tends to output the constant power P_{min} and the SC supports the rest power demand ($P_{demand}-P_{min}$). As shown in Fig. 8 (b), the DP

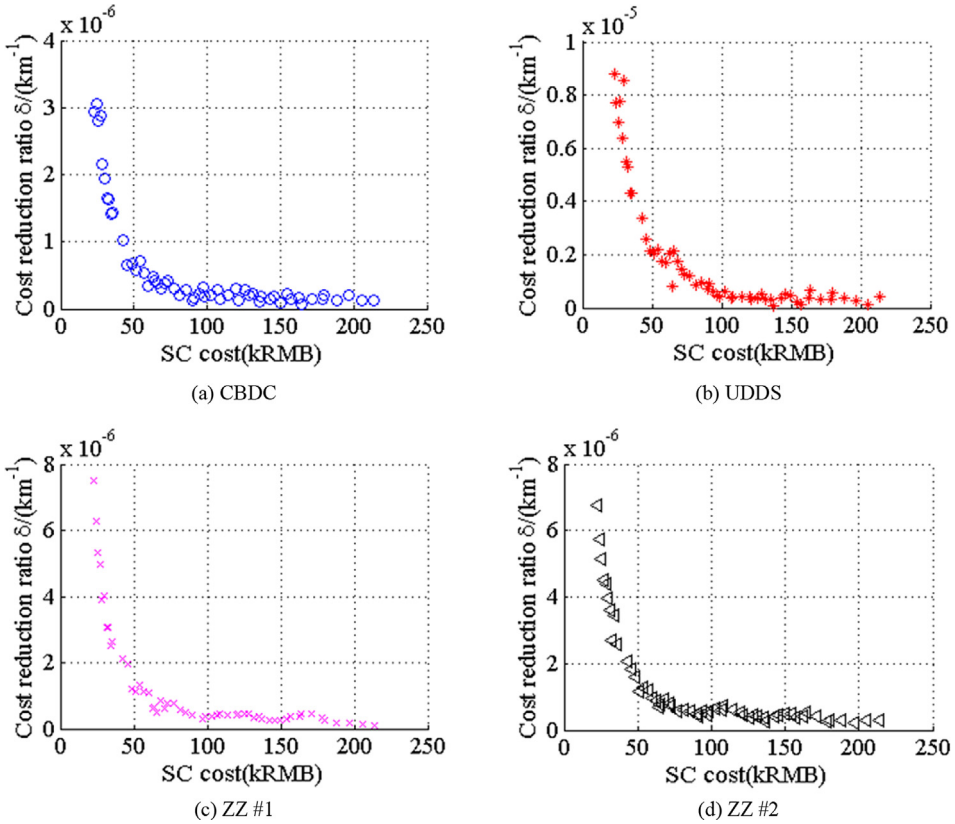

Fig. 7. The reduction rate δ results of different driving cycles.

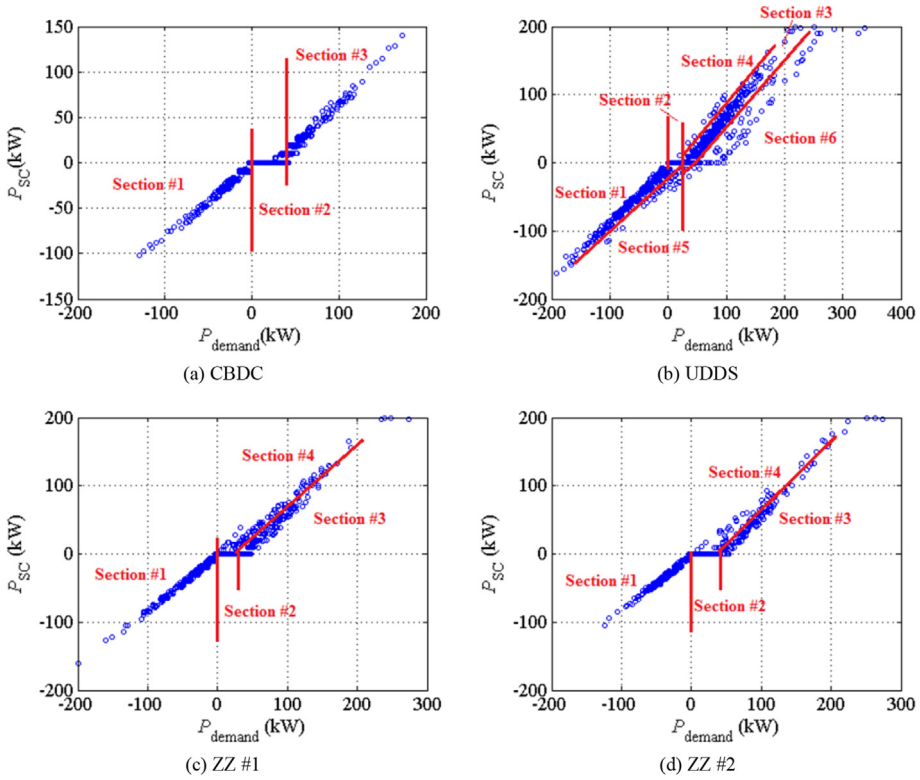

Fig. 8. The DP results of HESS along different driving cycles.

result under UDDS includes three new sections in addition to Section #1 to Section #3 when compared to the CBDC result. Section #4 reveals that the SC supplies power when P_{demand} is low. Section #5 implies that the battery should charge the SC even when P_{demand} is equal or more than 0 and V_{SC} is relatively high [6]. Section #6 indicates that the constant output power of the battery should be increased when the power demand P_{demand} is extremely high. Section #6 embodies the preparation of SCs through storing energy for the coming high power demand; in consequence, the SC can continuously work to relieve the battery stress when high power demand comes [6]. In fact, this characteristic cannot be taken into consideration in practical applications because the driving condition is random and difficult to predict. As shown in Fig. 7 (c) and (d), ZZ #1 and ZZ #2 have the similar result, which only contains Sections #1 to Section #4.

Actually, the characteristic of Section #4 only occurs in the end of the driving cycle and can be neglected. The reason is that the terminal SC voltage is unfixed in the DP process; therefore, the DP algorithm tends to drain the SC to reduce the battery degradation at the end of driving cycles. Among all driving cycles, only CBDC does not include Section #4 because its last micro-trip is intense (P_{demand} is high). In order to verify this conjecture, the DP process is conducted under two consecutive ZZ #1 cycles whose time duration is 1878s. The SC voltage during the entire time duration is shown in Fig. 9 (a), which shows that the SC is drained in the end of the DP process. In addition, the DP result from 0s to 1400s (only the last period is excluded) is shown in Fig. 9 (b), which only includes 3 sections. Hence, it is verified that the characteristic of Section #4 can be neglected. In addition, the simulation result also shows that time duration of the driving cycle has no significant influence on the optimization result.

In real-world applications, the battery is set to charge the SC with constant value P_{ch} when V_{SC} is less than 50% of its maximum value to protect the SC. Based on observations above, taking Section #1 to Section #3 into consideration, a rule-based EMS including 4 modes for on-line uses is proposed for CBDC, ZZ #1, and ZZ #2, as shown in Fig. 10.

Taking Section #1 to Section #3 and Section #6 into consideration, a rule-based EMS including 5 modes is designed for UDDS, as shown in Fig. 11. Where P_{hd} and P_{high} are two constant power values in the on-line EMS [6]. The above simulation results show that UDDS has remarkably different characteristics in both SC sizing and EMS optimization results when compared to the other driving cycles, since UDDS contains an intense micro-trip.

5.2. The influence of driving cycle on optimization results

As shown in Fig. 5, the λ distributions related to four driving cycles are different; however, the λ values of CBDC, ZZ #1, and ZZ #2 vary in the same range. Actually, the high-intensity micro-trip determines the optimal SC size and the structure of the on-line EMS, whereas the low-intensity micro-trip has slight influence on the optimization results. The 2nd micro-trip of UDDS has an extremely high intensity factor, which is 0.82 and much higher than the other micro-trips'. To verify this conclusion, the 2nd micro-trip in the UDDS can be removed, then examine the sizing result of the rest micro-trips. As shown in Fig. 12 (a), the optimal SC amount corresponding to the rest micro-trips of UDDS decreases from 72 (for the entire UDDS) to 50 (71.4 kRMB, $M_{SC} = 2$, and $N_{SC} = 25$), which is same to the solution of CBDC, ZZ #1, and ZZ #2 This is because the λ distribution of the rest micro-trips of UDDS (except the 2nd micro-trip) has a similar range with the ones of other driving cycles. In addition, the DP result under the rest micro-trips of UDDS (with optimal SC size: $M_{SC} = 2$, and $N_{SC} = 25$) is shown in Fig. 12 (b). It turns out that the relationship between P_{demand} and P_{SC} is simplified and can be divided into only Section #1 to Section #4, while

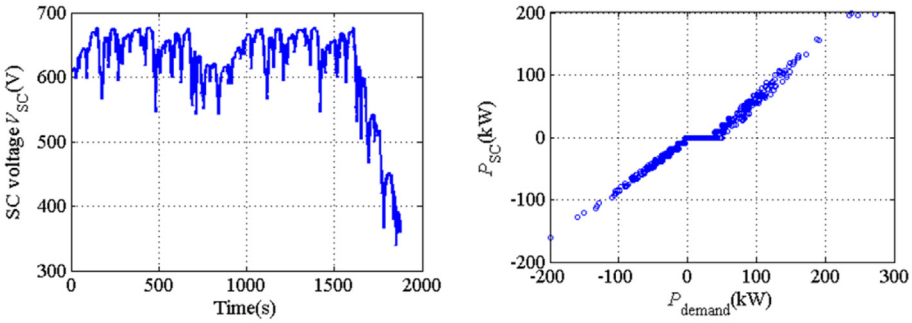

(a) The SC voltage curve (0s to 1878s) (b) The relationship of P_{demand} and P_{SC} (0s to 1400s)

Fig. 9. The DP result under two consecutive ZZ #1 cycles.

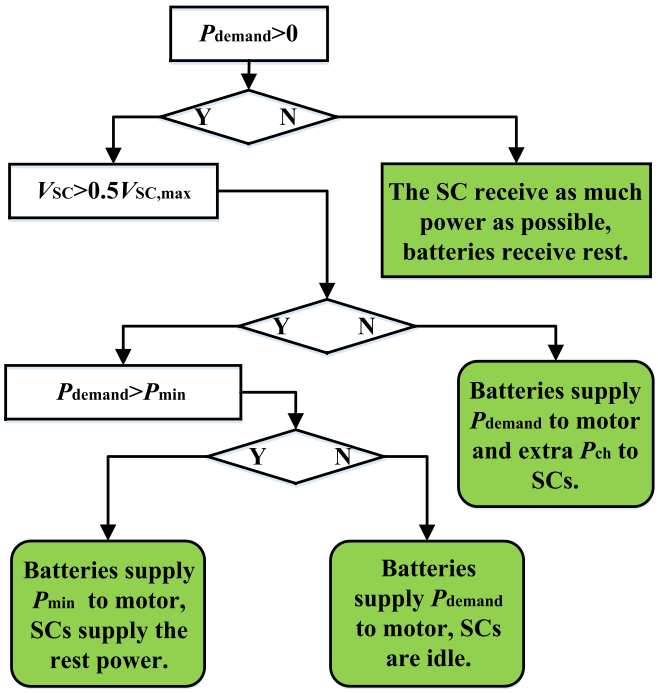

Fig. 10. The rule-based EMS for CBDC, ZZ #1, and ZZ #2.

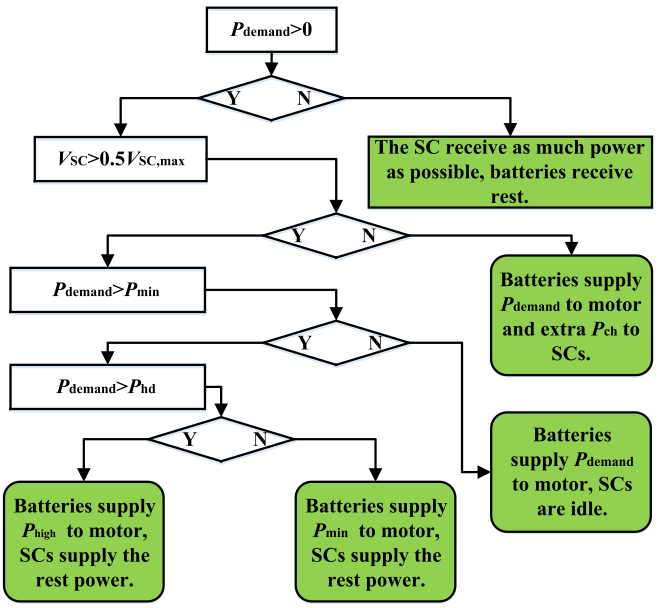

Fig. 11. The rule-based EMS for UDDS.

Section #5 and Section #6 disappear in the DP result. Thus the on-line EMS shown in Fig. 10 can be employed for the rest micro-trips of UDDS, which means that the 2nd micro-trip in UDDS dramatically influences not only the SC sizing result but also the optimal on-line EMS.

To further validate this conclusion, the ZZ #2 cycle is selected and modified. To be specific, the power profile of the 3rd micro-trip in ZZ #2 is increased to 2.5 times of its original values. The power profile and intensity factor distribution for the modified ZZ #2 are shown in Fig. 13. The intensity factor of 3rd micro-trip increases to 0.6742. Then the DP process is conducted under the modified ZZ #2, the optimization results are shown in Fig. 14. Compared to the sizing result shown in Fig. 7 (d), the optimal SC amount for the modified ZZ #2 is significantly increased from 50 to 66 (94.2 kRMB, $M_{SC} = 3$, and $N_{SC} = 22$). As shown in Fig. 14 (b), the DP result under the modified ZZ #2 should be divided into 6 sections, which means it needs the complex on-line EMS as shown in Fig. 11.

In conclusion, for different driving cycles, the optimal SC size and the on-line EMS are directly determined by the maximum intensity factor. The driving cycles with similar maximum intensity factors can adopt the same number of SC modules and employ the same on-line EMS. This criterion is convenient to optimize the HESS performance in practical applications because the DP process does not need to be repeated, which has high computational cost. Only the approximate driving data is required to derive the intensity distribution by using the proposed fuzzy pattern recognition. Furthermore, the complex integrated optimization is converted to the examination of the maximum intensity factor. The optimization result under the standard driving cycle can be easily generalized to the practical bus lines, which have similar maximum intensity factors.

6. Conclusion

This paper investigates the influence of different driving cycles on the integrated optimization of HESS, including the optimization of SC size and on-line EMS. The driving cycle is divided into micro-trips, and a fuzzy pattern recognition algorithm is proposed in this paper to extract the characteristic parameter of the micro-trip. The fuzzy pattern recognition algorithm has two inputs: the demand energy (the primary input) and the maximum discharge power (the auxiliary input), and one output: the intensity factor λ of micro-trip.

The integrated optimization of the HESS is conducted based on

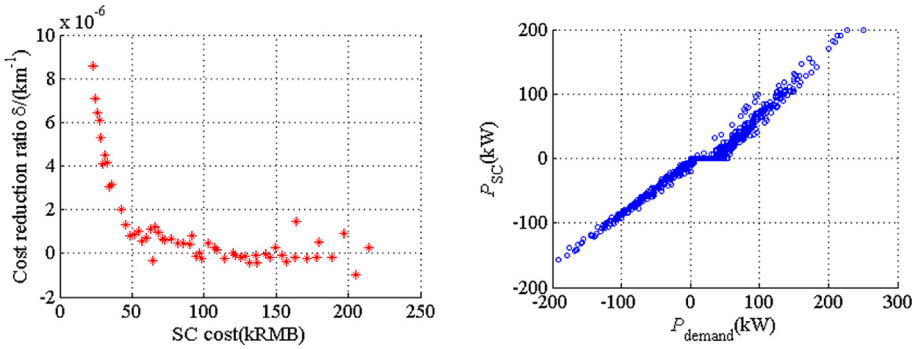

(a) Sizing result (b) The DP result

Fig. 12. The optimization result of UDDS when its 2nd micro-trip is removed.

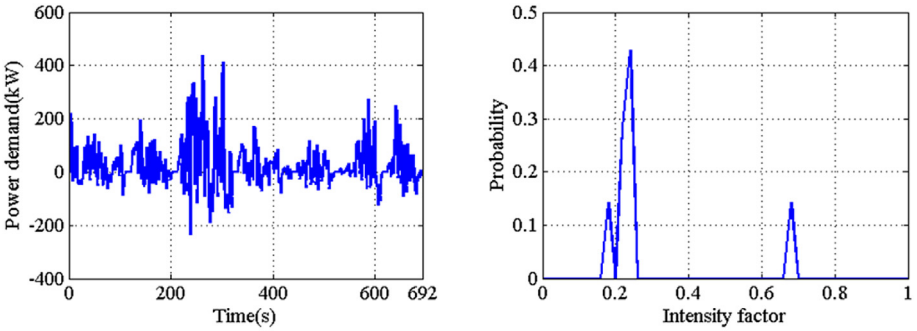

(a) Power profile (b) Intensity factor distribution

Fig. 13. The modified ZZ #2 cycle.

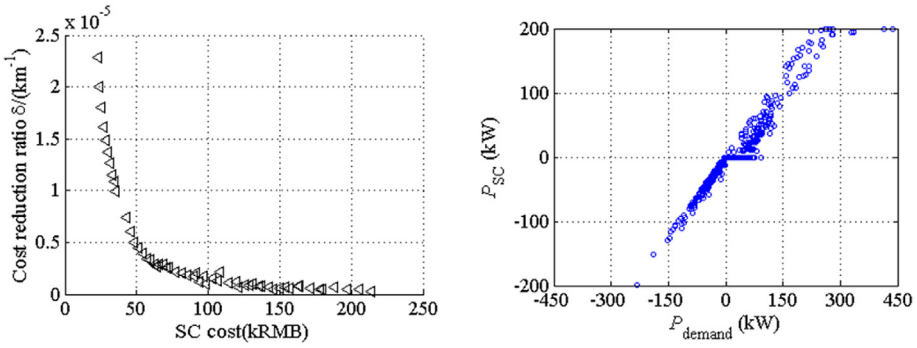

(a) Sizing result (b) The DP result (M_{SC} = 3, and N_{SC} = 22)

Fig. 14. The optimization result under the modified ZZ #2.

the four studied driving cycles (CBDC, UDDS, and two real bus driving cycles in Zhengzhou, China). The simulation results show that for different driving cycles, the optimal SC size and the on-line EMS are directly determined by the maximum intensity factor, which indicates how intensely the driving cycle drains energy from HESS. The driving cycles with similar maximum intensity factors can use same amount of SC modules and on-line EMS. This criterion can be used to optimize the HESS performance in practical applications because repeated conduction of the DP process, which has high computational cost, is avoided. Therefore, it is convenient to design the SC size and on-line EMS for EVs based on the driving cycle parameter. The complex integrated optimization is converted to the examination of the maximum intensity factor. Optimization results under standard driving cycles, including the SC sizing and on-line EMS design results, can be easily generalized to the practical bus lines as long as they have similar parameters because the influence of the driving cycle is inherently considered by the approach proposed in this paper.

Acknowledgement

This research is supported by National Science Foundation under Grant No. 51275264, and also supported by Ministry of Education (Research of distributed hybrid Powertrain for heavy duty trucks). The authors also want to thank Lecturer Christine Feak from the University of Michigan, Ann Arbor for revising the language of this manuscript.

References

[1] Ajanovic A, Haas R. Dissemination of electric vehicles in urban areas: major factors for success. Energy 2016;115:1451–8.

[2] Ichimura M, Shimomura M, Takeno K, Shirota R, Yakami J. Synergistic effect of charge/discharge cycle and storage in degradation of Lithium-ion Batteries for mobile phones. In: 27th International Conference on Telecommunications; Berlin, Germany, September, 2005.

[3] Deng Y, Li J, Li T, Zhang J, Yang F, Yuan C. Life cycle assessment of high capacity molybdenum disulfide lithium-ion battery for electric vehicles. Energy 2017;123:77–88.

[4] Song Z, Hou J, Hofmann H, Li J, Ouyang M. Sliding-mode and Lyapunov function-based control for battery/supercapacitor hybrid energy storage system used in electric vehicles. Energy 2017;122:601–12.

[5] Li J, Yang Q, Robinson F, Liang F, Zhang M, Yuan W. Design and test of a new droop control algorithm for a SMES/battery hybrid energy storage system. Energy 2016;118:1110–22.

[6] Song Z, Hofmann H, Li J, Han X, Ouyang M. Optimization for a hybrid energy storage system in electric vehicles using dynamic programing approach. Appl Energy 2015;139:151–62.

[7] Cao J, Emadi A. A new battery/ultracapacitor hybrid energy storage system for electric, hybrid, and plug-in hybrid electric vehicles. IEEE Trans Power Electron 2012;27:122–32.

[8] Destro N, Benato A, Stoppato A, Mirandola A. Components design and daily operation optimization of a hybrid system with energy storages. Energy 2016;117:569–77.

[9] Yu H, Tarsitano D, Hu X, Cheli F. Real time energy management strategy for a fast charging electric urban bus powered by hybrid energy storage system. Energy 2016;112:322–31.

[10] Wang Y, Liu C, Pan R, Chen Z. Modeling and state-of-charge prediction of lithium-ion battery and ultracapacitor hybrids with a co-estimator. Energy 2017;121:739–50.

[11] Yu H, Tarsitano D, Hu X, Cheli F. Real time energy management strategy for a fast charging electric urban bus powered by hybrid energy storage system. Energy 2016;112:322–31.

[12] Quiros DC, Thiruvengadam A, Pradhan S, Besch M, Thiruvengadam P, Demirgok B, et al. Real-world emissions from modern heavy-duty diesel, natural gas, and hybrid diesel trucks operating along major California freight corridors. Emiss Control Sci Technol 2016;2:156–72.

[13] Gong Q, Li Y, Peng ZR. Trip-based optimal power management of plug-in hybrid electric vehicles. IEEE Trans Veh Technol 2008;57:3393–401.

[14] Gu B, Rizzoni G. An adaptive algorithm for hybrid electric vehicle energy management based on driving pattern recognition. In: ASME 2006 International Mechanical Engineering Congress and Exposition. Chicago, USA, November 5-10; 2006.

[15] Jeon SI, Jo ST, Park YI, Lee JM. Multi-mode driving control of a parallel hybrid electric vehicle using driving pattern recognition. J Dyn Syst Meas control 2002;124:141–9.

[16] Lin CC, Peng H, Jeon S, Lee JM. Control of a hybrid electric truck based on driving pattern recognition. In: Proceedings of the 2002 Advanced Vehicle Control Conference, Hiroshima, Japan, September, 2002.

[17] Wu J, Zhang CH, Cui NX. Fuzzy energy management strategy for a hybrid electric vehicle based on driving cycle recognition. Int J Automot Technol 2012;13:1159–67.

[18] Langari R, Won JS. Intelligent energy management agent for a parallel hybrid vehicle-part I: system architecture and design of the driving situation identification process. IEEE Trans Veh Technol 2005;54:925–34.

[19] Wang J, Liu P, Hicks-Garner J, Sherman E, Soukiazian S, Verbrugge M, et al. Cycle-life model for graphite-LiFePO4 cells. J Power Sources 2011;196:3942–8.

[20] Masih-Tehrani M, Ha'iri-Yazdi MR, Esfahanian V, Safaei A. Optimum sizing and optimum energy management of a hybrid energy storage system for lithium battery life improvement. J Power Sources 2013;244:2–10. http://finance.sina.com.cn/money/forex/hq/USDCNY.shtml.

[21] Hao H, Ou X, Du J, Wang H, Ouyang M. China's electric vehicle subsidy scheme: rationale and impacts. Energy Policy 2014;73:722–32.

[22] Bata R, Yacoub Y, Wang W, Lyons D, Gambino M, Rideout G. Heavy duty testing cycles: survey and comparison. SAE Tech Pap 1994, 942263.

[23] Ansari M, Velusami S. DMLHFLC (Dual mode linguistic hedge fuzzy logic controller) for an isolated wind–diesel hybrid power system with BES (battery energy storage) unit. Energy 2010;35:3827–37.

[24] Petković D, Ćojbašić Ž, Nikolić V, Shamshirband S, Kiah M, Anuar N, et al. Adaptive neuro-fuzzy maximal power extraction of wind turbine with continuously variable transmission. Energy 2014;64:868–74.

[25] Song Z, Hofmann H, Li J, Han X, Zhang X, Ouyang M. A comparison study of different semi-active hybrid energy storage system topologies for electric vehicles. J Power Sources 2015;274:400–11.